ADVANCED FUNCTIONAL MATERIALS
www.afm-journal.de

High-Fidelity Bioelectronic Muscular Actuator Based on Graphene-Mediated and TEMPO-Oxidized Bacterial Cellulose

*Si-Seup Kim, Jin-Han Jeon, Hyun-Il Kim, Chang Doo Kee, and Il-Kwon Oh**

High-performance electoactive artificial muscles with biofriendly, biodegradable, and biocompatible functionalities have attracted enormous attention in the era of human friendly electronic devices such as wearable electronics, soft haptic devices, and implantable or disposal biomedical devices. Here, a high-fidelity bioelectronic soft actuator is reported based on biofriendly 2,2,6,6-tetramethylpiperidine-1-oxyl radical-oxidized bacterial cellulose (TOBC), chemically modified graphene, and ionic liquid [EMIM][BF_4] as plasticizer, thereby realizing large deformable, faster, biodegradable, air working, and highly durable TOBC-IL-G muscular actuator. Especially, the TOBC-IL-G(0.10 wt%) membrane shows a dramatic increment of the ionic conductivity up to 120%, of specific capacitance up to 95%, of tensile modulus up to 63%, and of tensile strength up to 60%, for TOBC-IL, resulting in 2.3 times larger bending deformation without serious back-relaxation phenomena. The developed high-performance and durable bioelectronic muscular actuator can be a promising candidate for satisfying the tight requirements of human-related bioengineering as well as biomimetic robotics and biomedical active devices.

1. Introduction

Some human friendly electronic products such as wearable electronics, mobile flexible displays, soft haptic devices, and implantable or disposal biomedical devices will require high-performance soft actuators[1–5] with biofriendly, biodegradable, and biocompatible functionalities. A promising candidate to satisfy these requirements in "greener" electronics[6] is to use electroactive bioorigin materials or naturally abundant functional biopolymers such as plant cellulose, cellulose acetate, chitosan, silk, and bacterial cellulose (BC). However, compared with synthetic ionic polymer actuators,[7–11] some biopolymer actuators[12–17] reported already in the open literature still have relatively low actuation performances.

Among electroactive biopolymers, BC has attracted significant interest due to its macromolecular structure, hydrophilic properties, higher crystallinity, dense reticulated structures, and strong mechanical properties, compared with other bioorigin materials, as well as its inherent biocompatible and biodegradable properties. Because of these unique properties, BC can be applied to a material source for biopolymer electrolytes with high electrochemomechanical properties in fuel cells.[18–20] Particularly, BC is cultivated using bacteria and is essentially an assembly of cellulose micro fibrils depending on hydrogen bonding and van der Waals interactions within and between cellulose molecules due to the presence of a large number of —OH radicals on the BC chains.[21] However, these characteristics are apt to form interfibrillar regions, thereby causing the fibers to entangle together tightly, resulting in a compound that is insoluble to all common solvents, including water. Our group very recently developed pure and freeze-dried BC-based actuators, but they showed relatively low actuation performance and poor durability, which inspired us to further investigate high-performance electroactive biopolymers.[13,22] Until now, BC-based artificial muscles with relatively high mechanical stiffness, low ionic conductivity, and actuation performance in comparison with those based on synthetic ionic polymers have not been improved by the reinforcement or functionalization of the BC biopolymer itself. To overcome the limitations of natural biopolymers for high-fidelity and durable actuations, two crucial issues should be resolved; 1) natural biopolymers should be chemically functionalized for much larger ion absorption and faster ion migration and structurally modified for mesoporous muscular structures and 2) flexible and stretchable electrodes having high electrical conductivity and capacitance should be integrated with chemical and physical compatibilities to the biopolymers.

Recently, many researchers have succeeded in the preparation of cellulose fibril dispersions based on dissociation of each cellulose micro fibril using a 2,2,6,6-tetramethylpiperidine-1-oxyl radical (TEMPO)-meditated oxidation procedure as one of several promising functionalization methods of BC.[21,23,24] Every one of two glucosyl residues of the cellulose chains in the surface

Dr. S.-S. Kim, H.-I. Kim, Prof. C. D. Kee
School of Mechanical Systems Engineering
Chonnam National University
77 Yongbong-ro, Buk-gu, Gwang-Ju 500-757,
Republic of Korea
J.-H. Jeon, Prof. I.-K. Oh
Graphene Research Center in KINC and Department of Mechanical Engineering
School of Mechanical and Aerospace Engineering
Korea Advanced Institute of Science and Technology (KAIST)
291 Daehak-ro, Yuseong-gu, Daejeon 305-338, Republic of Korea
E-mail: ikoh@kaist.ac.kr

DOI: 10.1002/adfm.201500673

of cellulose microfibril can be entirely oxidized to sodium glucuronosyl residues by TEMPO-mediated oxidation, resulting in the formation of sodium *carboxyl* groups on the microfibril surfaces with more surface area.[25] So, TEMPO-oxidized bacterial cellulose (TOBC) can be converted easily to individual nanofibrils in water, resulting in facile film formation using the casting method. Most interestingly in view of ionic actuators, the adoption of carboxylic groups instead of sulfonic groups through a TEMPO-mediated oxidization process can resolve the back-relaxation problem,[22] low response time and biocompatibility, one of the critical drawbacks of conventional ionic polymer actuators, due to the weakly polar carboxylic groups with weaker acidity, the smaller size of the carboxylic anion and better biocompatible properties as compared to those of sulfonic groups.[26] Also, the presence of carboxylic groups in BC allows it to be functionalized with bioactive molecules such as ionic liquid. But, the chemically functionalized TOBC derivatives having fascinating electrochemical properties needed for high-performance ionic artificial muscles have not been used until now.

In this work, we newly designed a high-fidelity bioelectronic artificial muscle utilizing biofriendly TOBC, chemically modified graphene, and ionic liquid [EMIM][BF_4] as plasticizer, thereby realizing large deformable, biodegradable, air working and highly durable TOBC-IL-G muscular actuator as shown in **Scheme 1**. Here, TOBC-IL-G means the graphene-reinforced TOBC membrane embedding ionic liquid. The carboxylic acid groups in TOBC, as a proton donator, can greatly contribute to higher ionic conductivity, higher ion exchange capacity (IEC), and higher capacitance and ionic liquid uptake ratio; these results from the provision of abundant protons, larger ion-exchange sites, larger surface area, and stronger interfacial coupling. The chemically modified graphene having functional groups plays a key role in enhancing mechanical stiffness, ionic conductivity, and capacitance of the nanobiocomposite. As a biofriendly, flexible and nonmetallic conducting electrode, poly(3,4-ethylenedioxythiophene) polystyrene sulfonate (PEDOT:PSS) treated with dimethyl sulfoxide (DMSO)[27] was deposited to top and bottom surfaces of the TOBC-IL-G membrane. The TEMPO treatment of BC, purification of chemically modified graphene, and plasticizing effect of IL can disrupt the aggregation of the BC composite matrix and make a well-dispersed biofriendly composite membrane, resulting in higher bending performance for TOBC-IL-G films, induced by a notable improvement in the electrochemical properties, tuned mechanical properties, and the electrochemical doping processes at the "green" PEDOT:PSS layers.[6,28–30]

2. Results and Discussion

2.1. Morphological Analysis

Figure 1 provides surface scanning electron microscope (SEM) images of pure TOBC, TOBC-IL, TOBC-G, and TOBC-IL-G composites, which confirm that the nanofibrous TOBC effectively and strongly binds with ionic liquid and chemically modified graphenes. These morphological features may be ascribed to the strong ionic interactions including electrostatic interaction and hydrogen bonding among the many carboxyl functional groups on the TOBC nanofibers, ionic liquids, and the functionalized chemically modified graphenes. So, it is evident that ionic liquids were first anchored on the surface of the TOBC nanofibers, and then the graphenes adhered to them as shown in Figure 1. The cross-sectional SEM morphologies (Figure S1, Supporting Information) of TOBC-IL and TOBC-IL-G composite films with different chemically modified graphene loadings (0.05 and 0.10 wt%) also exhibited fibrous network structures of ultrafine individual cellulose microfibrils, including well-embedded IL and randomly dispersed chemically modified graphenes, due to ionic interactions among TOBC, IL, and chemically modified graphene.[31] Therefore, the chemical structure of the TOBC-IL-G composite can be described as Figure 1, which contains the

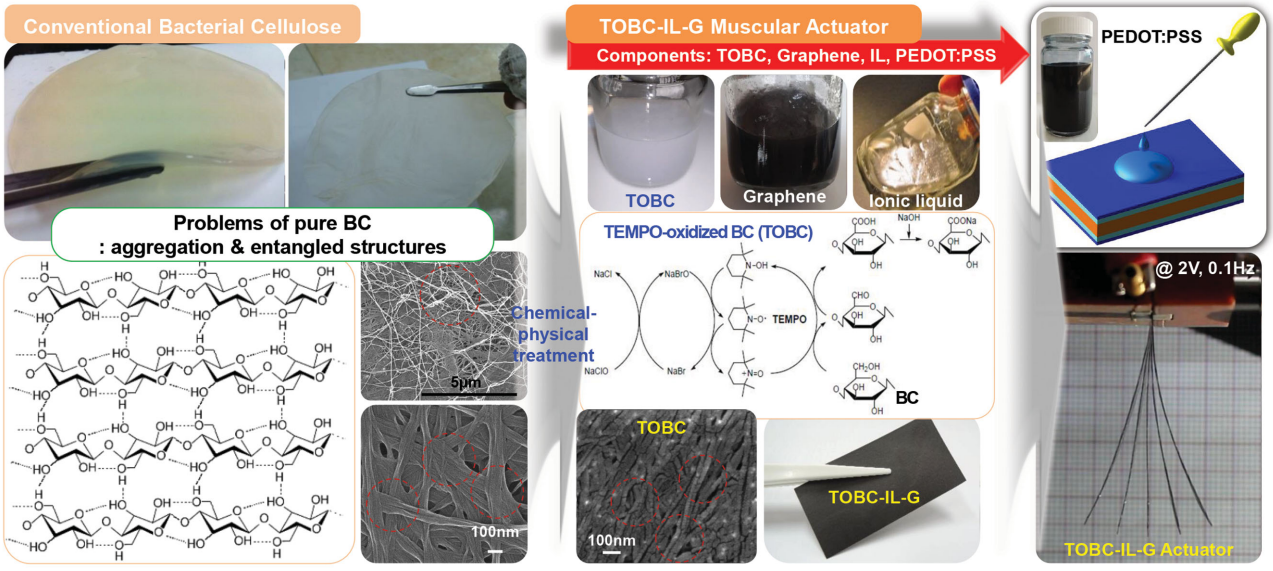

Scheme 1. Schematic illustration of bioelectronic TOBC-IL-G muscular actuator.

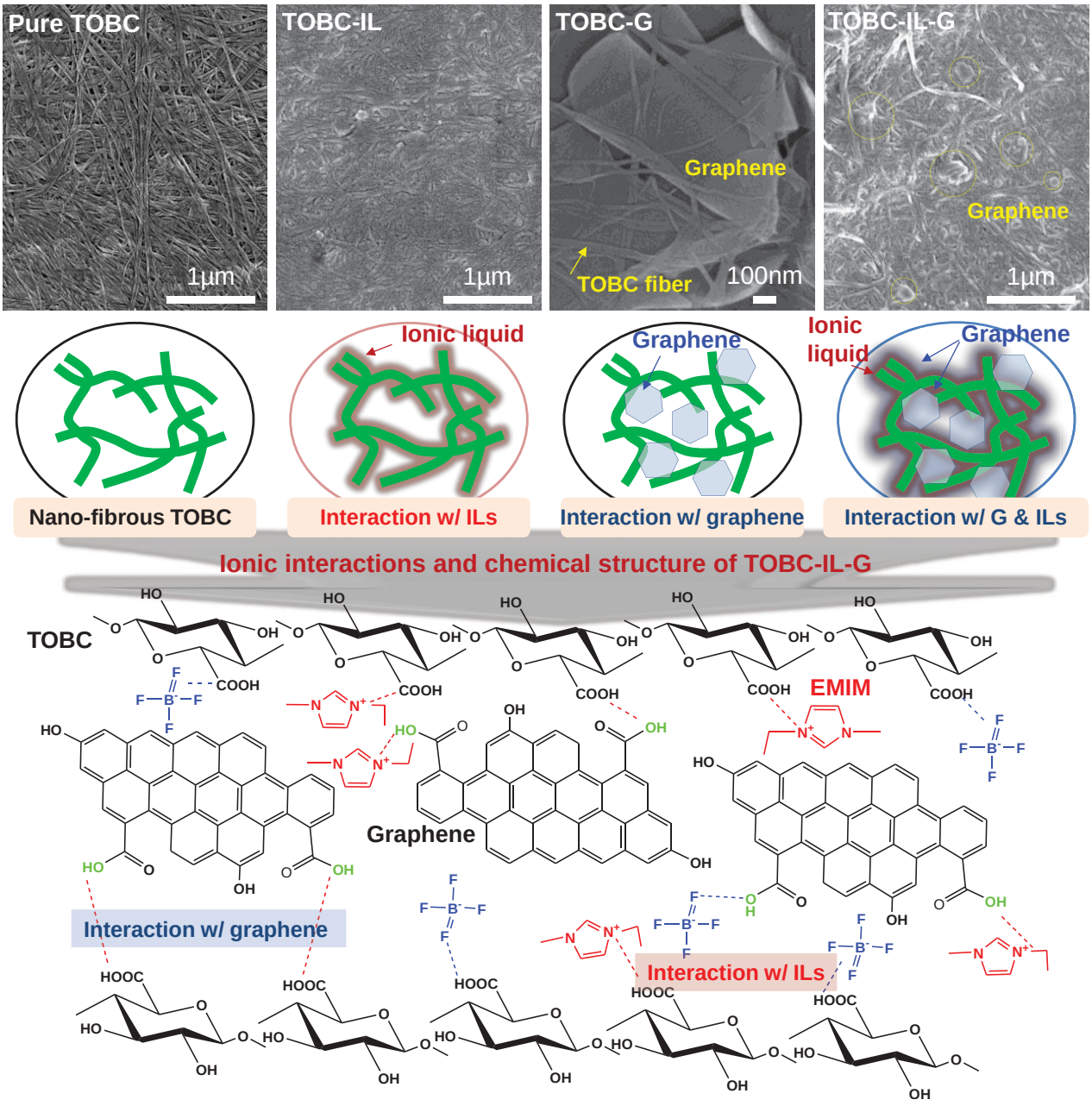

Figure 1. SEM images of pure TOBC, TOBC-IL, TOBC-G, and TOBC-IL-G and corresponding structural evolution and chemical structure of TOBC-IL-G membrane.

ionic interactions occurring among TOBC, IL, and chemically modified graphene; these interactions include the following: i) hydrogen bonding between TOBC and chemically modified graphene; ii) ionic crosslinking and ionic interaction of the IL (i.e., [EMIM][BF_4]) with the carboxylic and hydroxyl groups of TOBC and with —COOH and —OH of chemically modified graphene, resulting in tuned mechanical stiffness and enhanced interfacial compatibility of the TOBC-IL composite membrane. Furthermore, the well-dispersed TOBC-IL-G membranes exhibited color changes from gray to pale black due to the formation of nanocomposting between TOBC and chemically modified graphene. The color intensity gradually increased due to the loading level of the chemically modified graphene in the TOBC-IL matrix, and accompanying the π–π conjugation of chemically modified graphenes as shown in **Figure 2**.

2.2. Chemical Structures

Further, ionic interactions among TOBC, chemically modified graphene, and ionic liquid are confirmed by Fourier transform infrared spectroscopy (FT-IR) (**Figure 3**a–c). In the results for the TOBC membrane, the 3000–3600 cm^{-1} broad band, 2820–3000 cm^{-1}, and 1000–1175 cm^{-1} band indicate

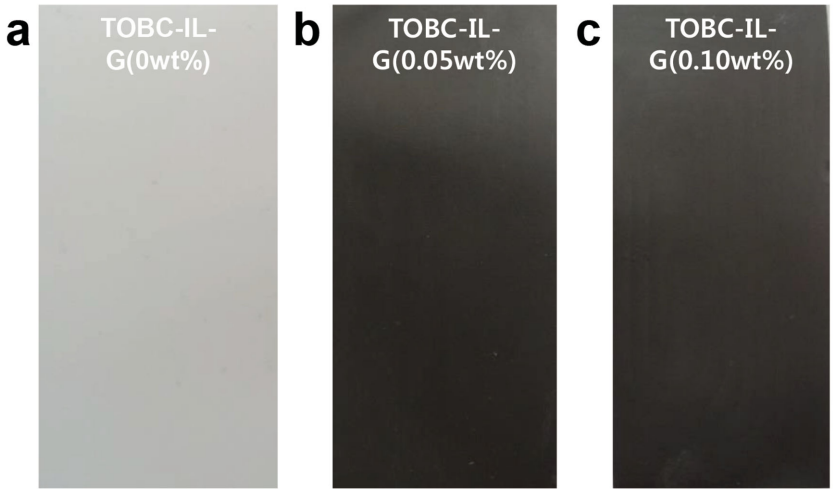

Figure 2. Colors of TOBC-IL-G composite membranes and ionic interactions with TOBC, IL, and graphene: a) TOBC-IL, b) TOBC-IL-G(0.05 wt%), and c) TOBC-IL-G(0.10 wt%).

the O—H stretching vibration, the aliphatic C—H stretching and the ether C—O—C bonding, respectively, as can be seen in Figure 3a.[32,33] In particular, the characteristic peaks of TOBC-IL appeared at 1605 cm^{-1} band, which indicates the C═O stretching of the carboxylic group evident in the TOBC and the enhanced intensity via the ionic interactions between the carboxylic group and the cation of the ionic liquid as distinctly shown in Figure 3b.[32,33] And the spectrum of TOBC-IL carried peaks at 3165 and 3120 cm^{-1}, and 750 cm^{-1} which correspond to C—H and BF_4 groups of neat [EMIM][BF_4], respectively. After TEMPO treatment, the absorbance of BC shifted from 1540 to 1605 cm^{-1}, indicating the presence of the carboxylic group in the bacterial cellulose. Thus, the results of FT-IR analysis clearly validate the formation of the anionic membranes with a fascinating carboxylic acid group and ionic interactions of TOBC-IL membranes. During the interaction between TOBC and the graphene nanoplatelets, these bands become much stronger due to the strong ionic interactions of the hydroxyl groups with chemically modified graphene nanoplatelets, as can be seen in the shape and strong band at 3410 cm^{-1} (ν_{OH}), shown in Figure 3c. Additionally, the thermogravimetric analysis (TGA), which indicates the thermal properties and stability of the TOBC-IL-G composite membranes, strongly supports the idea of ionic interactions and interfacial interactions of the TOBC with chemically modified graphene and IL, as shown in Figure 3d. They undergo decomposition in three stages; the first stage involves evaporation of water molecules and remnant solvent at 0–200 °C; the second corresponds to the decomposition of bacterial cellulose at 250–370 °C; and the third stage involves the vaporization and elimination of residual volatile compounds. After TEMPO treatment, the thermal stability of TOBC decreased due to the disruption of aggregation of the BC composite matrix and the presence of weakly polar carboxylic groups in the TOBC matrix. On the other hand, after reinforcement of graphene and ionic liquid, the thermal stability of TOBC-IL-G bionanocomposties were enhanced due to strong ionic interactions and interfacial interactions of the TOBC with graphene and ionic liquid.

2.3. Mechanical Properties

The mechanical properties of the composite membranes were evaluated through typical tensile test as shown in **Figure 4**a; the determined mechanical properties are compared in **Table 1**. The tensile modulus decreased from BC to TOBC due to the formation of individual cellulose nanofibrils, resulting from reductions of aggregation and of entangled structures. In particular, the proposed TOBC-IL composite membrane incorporating IL by ionic interaction displays an exceptionally superior elongation, up to ≈20%, which is much better than that of pure BC and TOBC membranes. On the other hand, the TOBC-IL-G(0.10 wt%) composite showed a dramatic increment of tensile modulus, up to 63%, and of tensile strength up to 60%, for TOBC-IL. The results indicate that the TOBC was further strengthened by the graphene; TOBC exhibits a tuned mechanical stiffness and higher mechanical strength compared to those of pure TOBC and TOBC-IL membranes without chemically modified graphene loading. Thus, the consistency indicates the good dispersion of chemically modified graphenes and [EMIM][BF_4] in the TOBC biopolymer matrix due to electrostatic interactions and hydrogen bonding among functionalized TOBC, graphene, and IL. As a result, the overall tensile stiffness of the TOBC-IL-G membrane was properly tailored compared with that of the pure TOBC membrane. And, the variations of the semicrystallinities of the pure TOBC, TOBC-IL, and TOBC-IL-G with ionic clusters were confirmed by X-ray diffraction (XRD) pattern analysis (Figure 4b). Characteristic peaks at 2θ = 14.3°, 17.02°, and 22.9° are observed in the case of pure TOBC; these correspond to the typical features of BC, which has crystalline and amorphous regions. For TOBC with chemically modified graphene composite, peaks are still observed, while the pronounced (0 0 2) peaks and (0 0 4) peaks of graphene nanoplatelets are observed at 2θ = 26.5° and 54.6°, respectively. The peaks of the X-ray diffractogram show not only that the TOBC with graphene composite maintained the features of BC but also that the characteristic graphitic peak intensity amplified with the higher chemically modified graphene loading.

2.4. Electrochemical Properties

The IEC of the membranes plays a crucial role in any evaluation of the ionic liquid uptake and the ionic conductivity. A highly ionic conducting fibrous networked muscular matrix can strongly affect the electrochemomechanical properties, such as IEC, ionic liquid uptake, ionic conductivity, tensile modulus, and tensile strength listed in Table 1 due to more numerous ionic interactions and stronger interfacial coupling between the ionic liquid and the chemically modified graphene reinforced TOBC. The IEC values of the TOBC, TOBC-G(0.05 wt%), and TOBC-G(0.10 wt%) membranes are 1.51, 1.56, and 1.63 meq. g^{-1}, respectively; the ionic liquid uptake values of

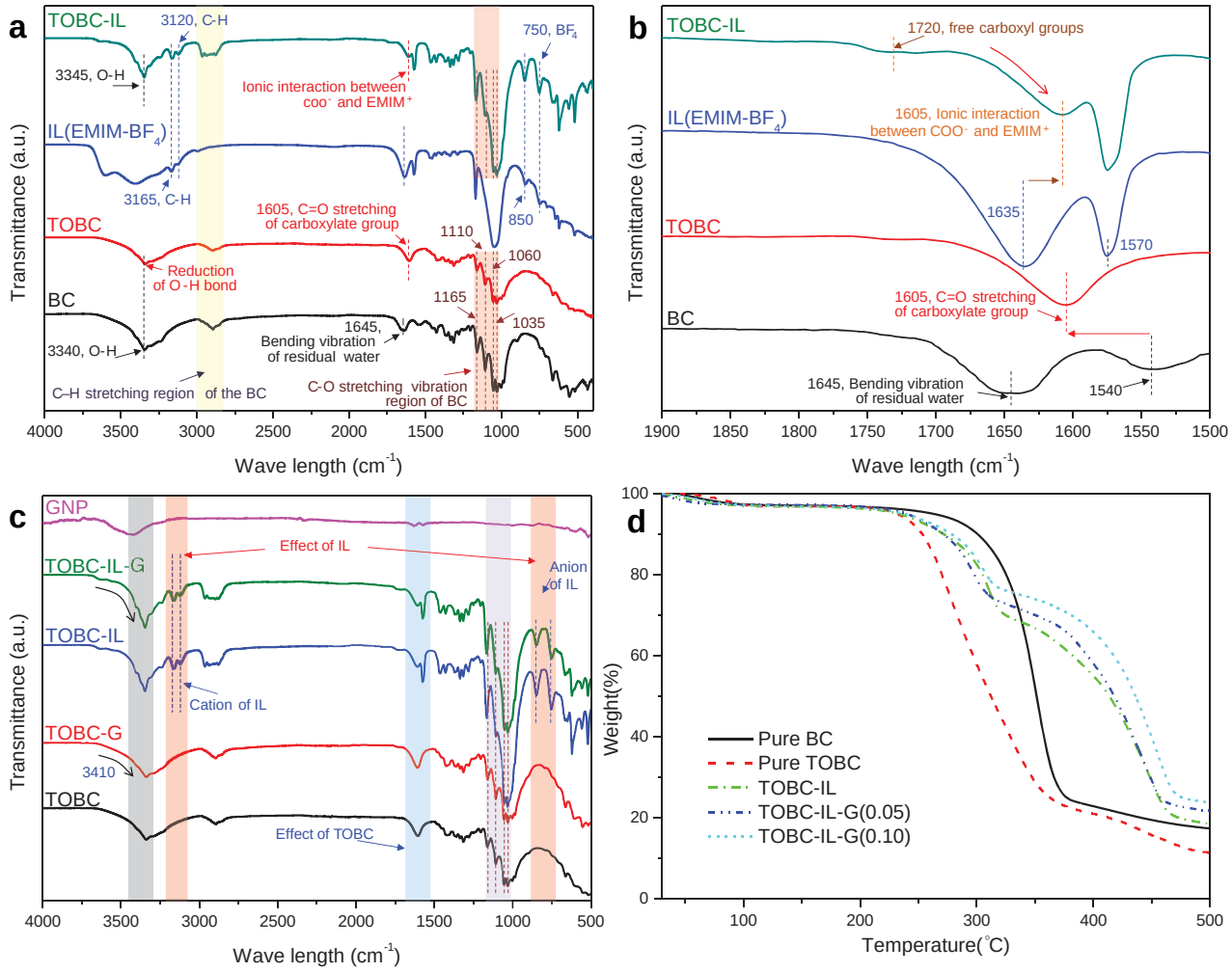

Figure 3. Chemical and thermal properties of TOBC-IL-G biocomposite membrane: a) FT-IR spectra ranging from 400 to 4000 cm^{-1}, b) from 1500 to 1900 cm^{-1} of BC, TOBC, IL and TOBC-IL, c) FT-IR spectra of TOBC-G and TOBC-IL-G, and d) TGA curves of TOBC-IL-G biocomposite membrane.

the TOBC, TOBC-G(0.05 wt%), and TOBC-G(0.10 wt%) membranes were 34.82%, 40.95%, and 48.47%, respectively, because of the functional groups of TOBC and chemically modified graphene, and their high interfacial interactions with ionic liquid. Additionally, we measured the specific capacitance of all three TOBC-IL-G membranes with different loading levels of graphene for considering the charge dynamics and the interfacial coupling inside the composite matrix. The specific capacitances of TOBC-IL-G(0.10 wt%), TOBC-IL-G(0.05 wt%), and TOBC-IL membranes were found to be 72.48 μF cm^{-2} (2.115 mF g^{-1}), 43.32 μF cm^{-2} (1.356 mF g^{-1}), and 37.13 μF cm^{-2} (0.975 mF g^{-1}) under ±2.0 V peaks at a scan rate of 100 mV s^{-1}, respectively. The TOBC-IL-G(0.10 wt%) membranes, which has the largest specific capacitance, are suitable for the polyelectrolyte of a high-performance ionic polymer actuator. Furthermore, **Figure 5** shows the specific capacitance and cyclic voltammetric (CV) curves of TOBC-IL-G bionanocomposties actuators with PEDOT:PSS electrdoes to characterize the effect of chemically modified graphene on the TOBC-IL-G actuators using cyclic voltammetry tests. The measured specific capacitances of TOBC-IL-G(0.10 wt%) (41.106 mF cm^{-2}) and TOBC-IL-G(0.05 wt%) (32.487 mF cm^{-2}) actuators are larger than those of the pure TOBC-IL (21.364 mF cm^{-2}) actuator under ±2.0 V peaks at a scan rate of 50 mV s^{-1}. Especially, the specific capacitance of TOBC-IL-G(0.01) is superior to that of TOBC-IL at various scan rates (Figure 5a–c). As the scan rate increases from 50 to 200 mV s^{-1}, the specific capacitance of all three TOBC-IL-G composites actuators decreases. Especially, the roughly rectangular shape, i.e., capacitive hysteresis behavior, indicates the good charge propagation within the TOBC-IL-G matrix and that matrix's capacitive-like behavior as shown in Figure 5d.

2.5. Actuation Performance

To evaluate the actuation performances of the dry-type TOBC-IL-G muscular actuator in open air, electrical harmonic, and step input signals was applied to both PEDOT:PSS electrode layers. **Figure 6**a shows the harmonic responses of the TOBC-IL-G actuators. Under sinusoidal excitation of 1.0 V at 0.1 Hz, the tip displacement of the TOBC actuator reached a peak of ±1.2 mm, while, for the TOBC-IL-G actuators, peak tip displacements

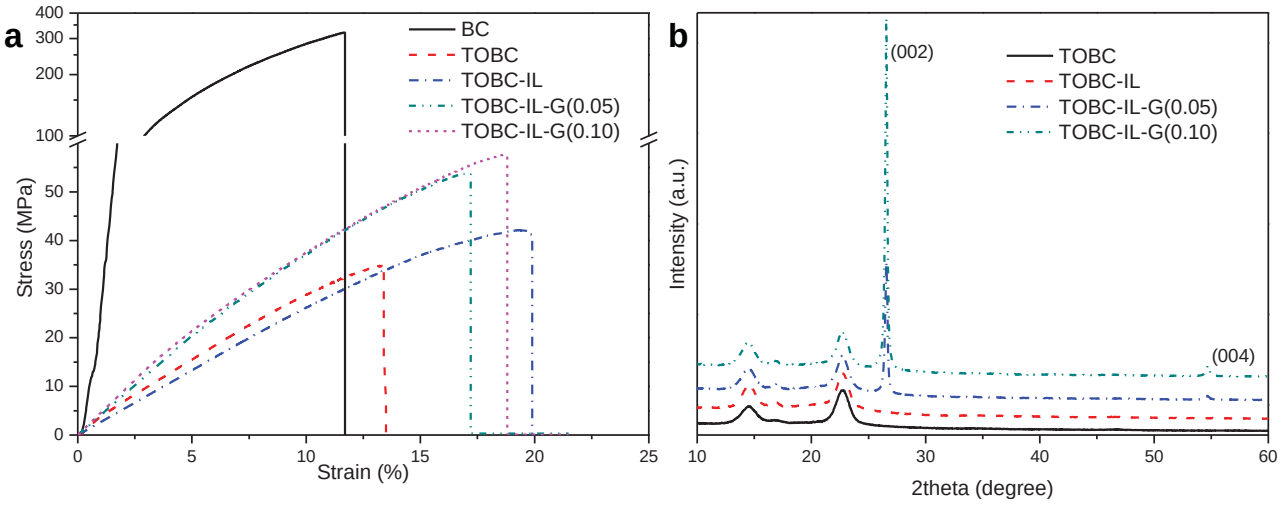

Figure 4. Mechanical and structural properties of TOBC-IL-G biocomposite membrane: a) tensile curves of BC and TOBC-IL-G composite membranes and b) XRD curves of TOBC-IL-G composite membranes.

were of ±2.5 and ±4 mm. The experimental results demonstrate that the TOBC-IL-G actuator shows much larger bending actuation than that of the TOBC actuator. Also, the response times were greatly improved due to the higher electrochemomechanical properties compared with those of pure BC-IL and TOBC-IL actuators. As illustrated in Figure 6b, the tip displacements of the TOBC-based actuators are 3.5, 5.1, and 6.3 mm, without the back-relaxation phenomenon that stems from the weakly polar carboxylic groups in the TOBC matrix. This higher bending performance of the newly developed TOBC-IL-G composite actuator is induced by the higher ionic conductivity, lager specific capacitance, and tuned mechanical properties, all of which result from the strong ionic interactions among the carboxylic groups of TOBC, chemically modified graphene, IL, and PEDOT:PSS, and from the ionic conducting fibrous muscular matrix. These factors led to increased ionic liquid absorption, which in turn led to easy and fast ion transport within the nanocomposite matrix, thereby offering the capability to enhance the bending actuation performance.

Additionally, peak-to-peak displacements and strains were evaluated under a sinusoidal electrical wave of ±1.0 and ±2.0 V peaks and excitation frequency of 0.1 Hz, as shown in Figure 6c. The degree of electromechanical deformation is strongly affected by the applied voltage due to high dependence of ionic mobility on the electric potential field in the nanocomposite matrix. Peak-to-peak displacements of the TOBC-IL-G actuator at ±1 V remarkably reach up 4.0 mm. Most importantly, the TOBC-IL-G actuator exhibited a durable actuation performance without a performance degradation for 3 h under continuous sinusoidal electrical wave of ±1.0 peak voltage at 0.5 Hz frequency. After an actuation test of 180 min, the actuator still exhibits a very harmonic response without performance degradation and response distortion (inset of Figure 6d). It is thought that this was due to the synergistic effects of the unique ionic conducting fibrous networked structure and the strong ionic interactions among the IL, chemically modified graphene, carboxylic acid groups in the nanochannels of TOBC, and PEDOT:PSS. The enhancement of the specific capacitance and the nonfaradaic behavior are confirmed in Figure 5a–d, respectively.

The actuation mechanism of the conducting polymer actuators is well known as doping/dedoping processes based

Table 1. Electrochemomechanical properties of TOBC-G-IL composite membranes.

Membrane	IEC [meq. g^{-1}]	IL uptake/swelling ratio	Capacitance [$\mu F\ cm^{-2}$/$mF\ g^{-1}$]	Tensile modulus [GPa]	Tensile strength [MPa]	Elongation [%]	Ionic conductivity [$S\ cm^{-1}$]
BC	1.15			3.145 ± 0.182	283.04 ± 42.67	11.04 ± 0.56	8.14×10^{-6}
BC-IL	–	27.34/11.63		–	–		1.04×10^{-4}
TOBC	1.51	34.82/17.97		0.469 ± 0.031	39.68 ± 4.94	14.82 ± 1.33	$1.59 \times 10^{-3a)}$
TOBC-G(0.05 wt%)	1.56	40.95/20.97		–	–		$2.26 \times 10^{-3a)}$
TOBC-G(0.10 wt%)	1.63	48.47/24.49		–	–		$3.72 \times 10^{-3a)}$
TOBC-IL	–	50.0	37.13/0.975	0.353	43.36	18.81	2.04×10^{-4}
TOBC-IL-G(0.05 wt%)	–	50.0	43.32/1.356	0.479	62.02	19.37	3.10×10^{-4}
TOBC-IL-G(0.10 wt%)	–	50.0	72.48/2.115	0.576	69.46	19.73	4.50×10^{-4}

[a)]These values were measured in fully hydrated condition.

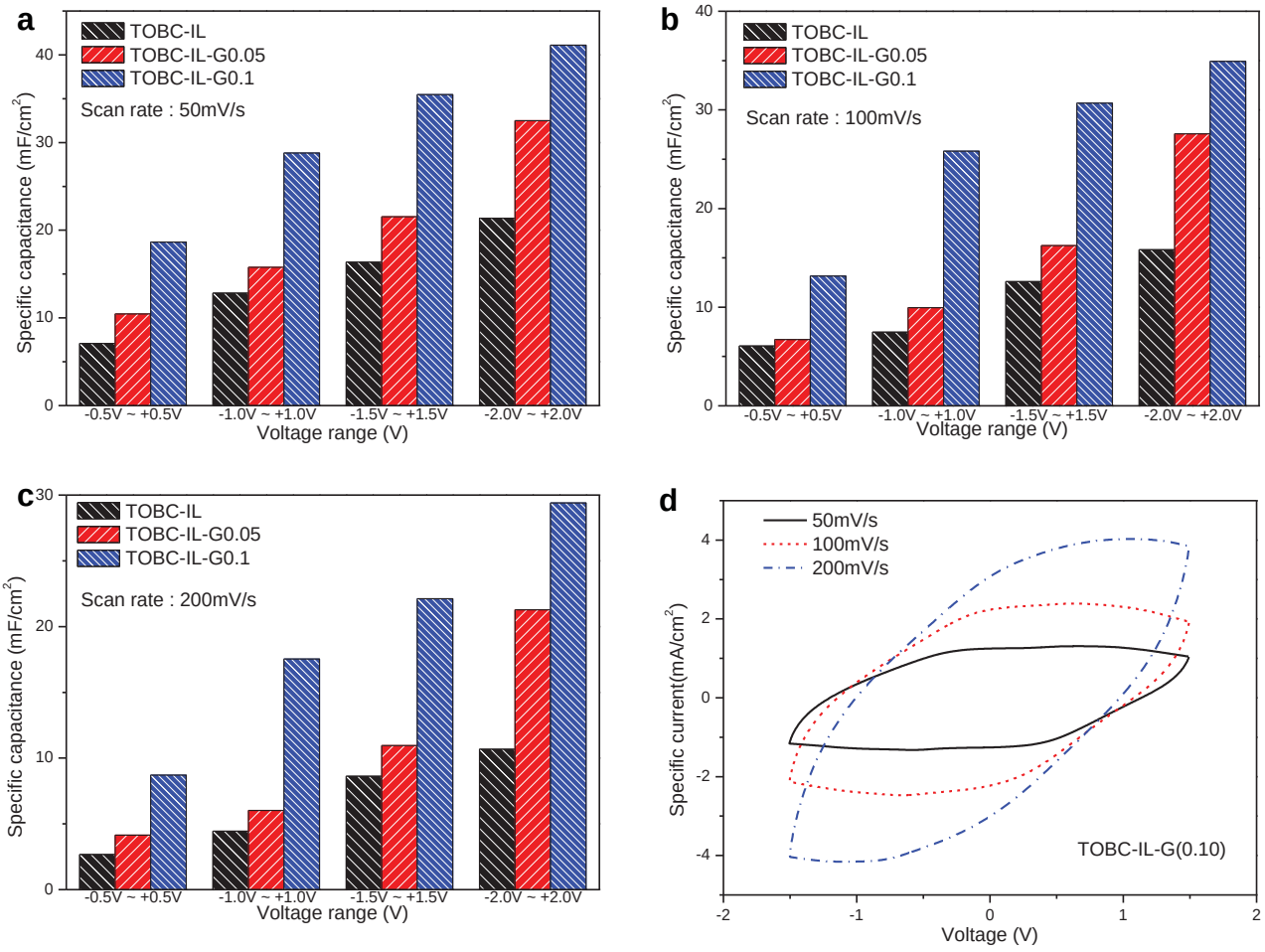

Figure 5. Specific capacitance and CV curves of TOBC-IL-G actuator according to scan rate: a) 50 mV s^{-1}, b) 100 mV s^{-1}, c) 200 mV s^{-1}, and d) current–voltage curves of TOBC-IL-G composite actuator at various scan rates.

on electrochemical redox reaction.[22] When an input voltage is applied between two conducting polymer PEDOT:PSS layers of the actuator, the potential difference between the PEDOT:PSS electrode layers induces the formation of the $PEDOT^+$-PSS^- ion pairs via the electrochemical doping process, and simultaneously leads to the absorption of cations or anions of the dissociated ionic liquid into the PEDOT:PSS electrode layer and to the emission of counter ions from the other layer as Equations (1) and (2). As a result, the actuator was bent by the differential expansion of the PEDOT:PSS layer at the anode electrode, an electrochemical reduction process between PEDOT:PSS and imidazolium that occurred according to the chemical Equation (1), respectively. Thus, the bending of the actuator is induced by the differential expansion of the PEDOT:PSS layer during the chemical doping process of the PEDOT:PSS electrodes and the bending actuation direction is simultaneously the same as that during the ionic migration inside the TOBC-IL-G composite membrane. In the anode electrode, an electrochemical reduction will occur according to the following process: The $PEDOT^+$ network provides the conduction path, obtained from the PEDOT:PSS layer which contains p-doped $PEDOT^+$ and PSS^- oligomer chain. Electron injection into the PEDOT:PSS layer can reduce it to $PEDOT^0$. At this stage, it shows comparatively low conduction due to the formation of a PEDOT zero oxidation state. Simultaneously, the dissociated cations obtained from both [EMIM][BF_4] and the TOBC membrane are involved in ionic bonding with PSS anions under strong electric field that produce a large amount of swelling at the anode. Also, in the cathode electrode, an electrochemical oxidation will occur according to the following process. The anions (i.e., BF_4^-) obtained from both [EMIM][BF_4] and the TOBC membrane strongly interact with the cathodic PEDOT:PSS layer and they can bind ionically with $PEDOT^+$ cations. As a result, swelling occurs at the cathode. The anion injection into the PEDOT:PSS layer can oxidize n-doped PSS^- to become the neutral PSS^0, as in Equation (2).[34–36] However, the molecular size of the cations is larger than their counterparts, which reflects the direction of the bending actuation mechanism of the designated sandwich PEDOT:PSS-TOBC composite-PEDOT:PSS electrode. Significantly, the proposed novel electrode showed enhanced bending deformation under harmonic and step inputs as compared to the TOBC-IL-G membrane. The total actuation mechanism includes electrochemical doping processes and ion migrations of dissociated ionic liquids under an electric potential field;

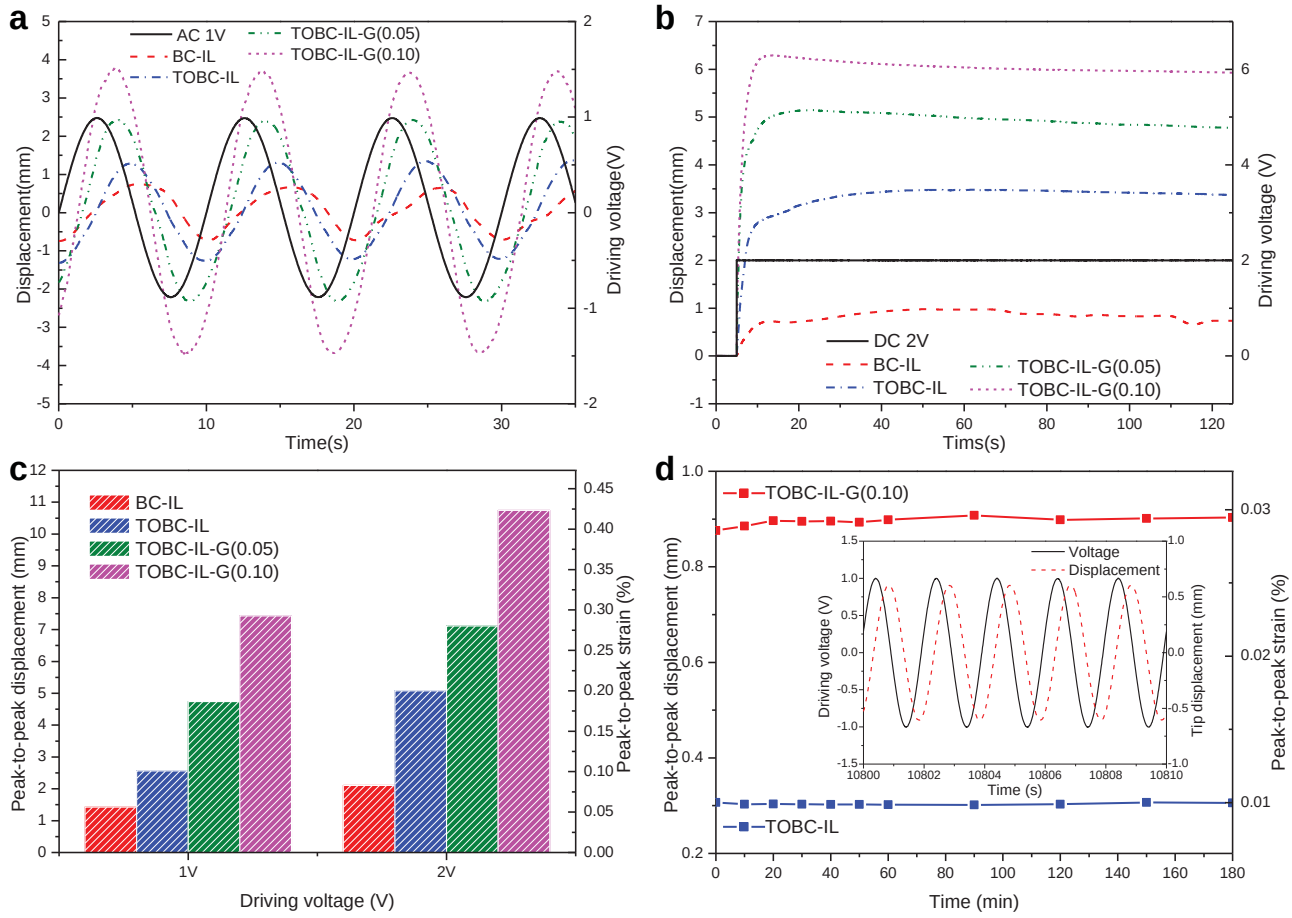

Figure 6. Actuation performances of TOBC-IL-G muscular actuators: a) harmonic responses under sinusoidal excitation of 1.0 V at 0.1 Hz, b) step responses under DC 2 V, c) peak-to-peak displacements and strains at different voltages, and d) durability results.

this overall process shows synergistic effects for much larger bending deformation of the TOBC-IL-G actuator.

$$PEDOT^{n+}:PSS^{n-}+m\mathrm{EMIM}^{+}+me^{-}\leftrightarrow PEDOT^{(n-m)+}:PSS^{(n-m)-}+mPDEOT^{0}+m\left(\mathrm{EMIM}^{+}:PSS^{-}\right) \quad (1)$$

$$PEDOT^{n+}:PSS^{n-}+m\mathrm{BF}_4^{-}\leftrightarrow PEDOT^{(n-m)+}:PSS^{(n-m)-}+mPSS^{0}+m\left(PEDOT^{+}:\mathrm{BF}_4^{-}\right)+me^{-} \quad (2)$$

As can be seen in the results of the step and harmonic responses, the higher specific capacitance values of the TOBC-IL-G actuators (Figure 5) cause much larger tip displacement and improvement in the response, seen in the rising time, the phase delay, etc. And, the ionic conductivities of the TOBC-IL-G membrane are enhanced by adding chemically modified graphenes from 2.04×10^{-4} to 4.50×10^{-4} S cm^{-1}, as listed in Table 1. **Figure 7** shows the large deformed shapes with converged constant curvature of the TOBC-IL-G(0.10 wt%) muscular actuator under DC 2.5 V, without showing back-relaxation phenomenon. The tip displacement of the as-fabricated actuator exceeded half the value of the displacement sensor within 1 s; it continued to deform with a converged constant curvature at very rapid speed in the following 5 s interval. Relatively fast response and large deformation of the TOBC-IL-G(0.10 wt%) muscular actuator at relatively higher step excitation were observed. Also, the deformation was maintained steadily under the quasi-static excitation due to effective ionic liquid migration within the ionic networked TOBC-IL-G membrane having fascinating carboxylic groups of TOBC and functional groups of chemically modified graphenes. Also the TOBC-IL-G(0.10 wt%) muscular actuator shows the large deformed shapes under harmonic excitation as shown in Figure S2 (Supporting Information).

3. Conclusion

In summary, we have developed a high-performance bioelectronic artificial muscle, so called TOBC-IL-G actuator, based on TEMPO-oxidized bacterial cellulose and chemically modified graphene, ionic liquid, and DMSO-doped PEDOT:PSS. Due to many carboxyl and hydroxyl functional groups in the TOBC units, synergistic ionic interactions among TOBC, graphene, and IL, including electrostatic interaction and hydrogen bonding, greatly enhance the electrochemical properties such as ionic conductivity, IEC, and capacitance and IL uptake and

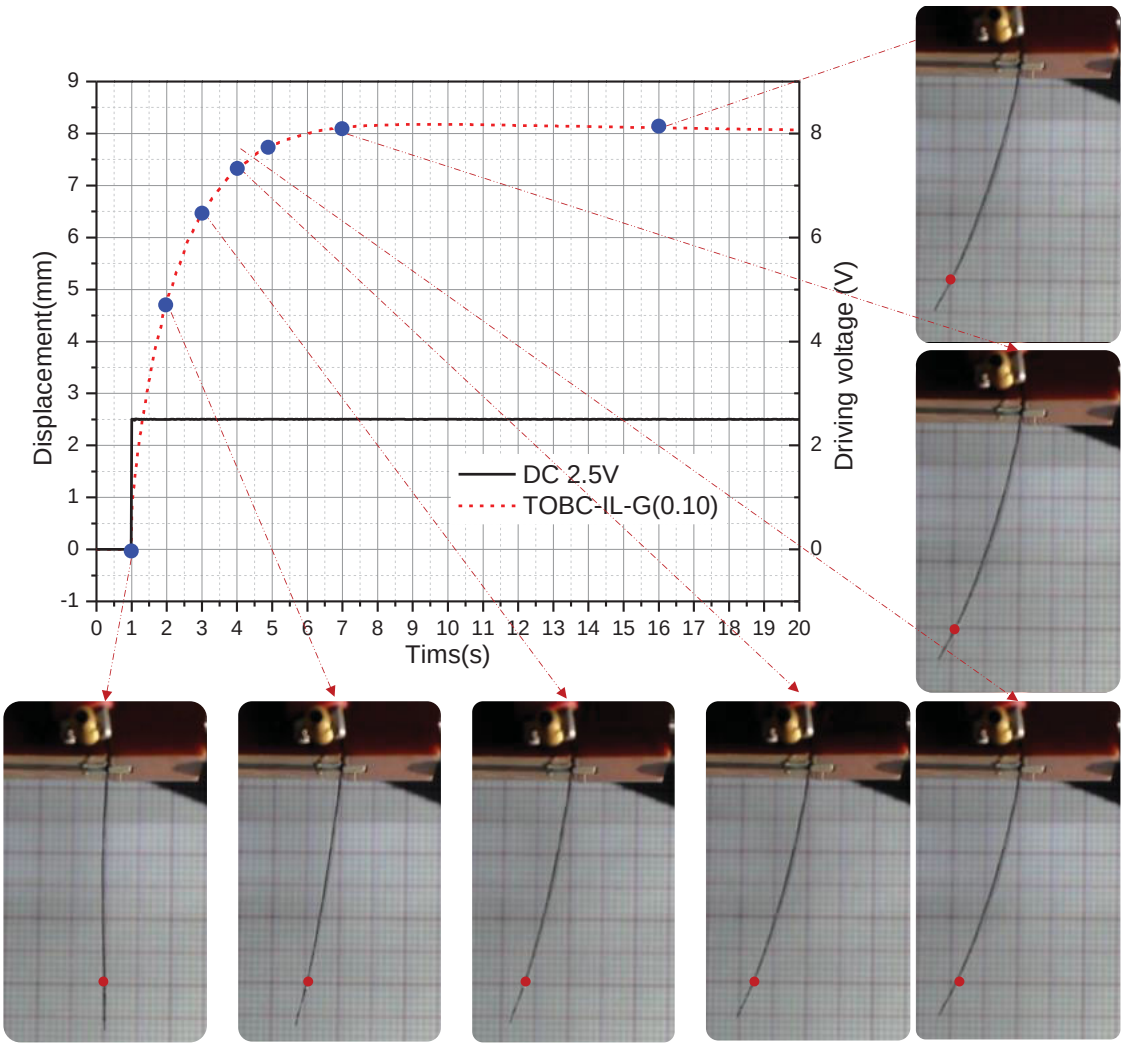

Figure 7. Electromechanically deformed shapes of TOBC-IL-G muscular actuator under a step input with DC 2.5 V.

remarkably strengthen mechanical stiffness of the TOBC-IL-G membrane, resulting in a dramatic increment of tensile modulus up to 23% and of tensile strength up to 75%, compared with pure TOBC. The unique TOBC-IL-G muscular actuator having biodegradable and biofriendly functionalities shows exceptionally large static deformation without apparent back-relaxation, much faster response time and highly durable harmonic actuation compared with conventional biopolymer actuators. Moreover, all used materials are abundant, inexpensive, and biofriendly, so the TOBC-IL-G muscular actuators can be used in human friendly electronic products such as wearable electronics, mobile flexible displays, soft haptic devices, and implantable or disposal biomedical devices requiring high-performance soft actuators with biofriendly and biodegradable functionalities.

4. Experimental Section

TEMPO-Mediated Oxidation of BC: TEMPO-mediated oxidation was applied to BC[13,37] produced by static culture using Hestrin and Shramm medium with sodium hypochlorite (NaClO), TEMPO and sodium bromide (NaBr) according to the previously reported method.[25,32] The BC pellicles (1 g) were suspended into deionized water (100 mL) containing TEMPO (0.016 g, 0.1 mmol) and NaBr (0.1 g, 1 mmol) under stirring. The 12% NaClO solution (3.1 g, 5.0 mmol) was slowly added to the BC slurry under gentle agitation at room temperature. The pH of the slurry was adjusted to ≈10 by adding 0.5 M NaOH solution. The TOBC was then filtered and washed with deionized water for several times. Finally, TOBC dispersion was obtained by adding 0.45 g TOBC to the deionized water (100 mL) under stirring. The TOBC had a carboxylate content of 1.3 mmol g^{-1}, i.e., 22.1% of C_6-OH groups in the BC were converted to sodium C_6-carboxylate groups, which was determined using the conductivity titration method.[38]

Preparation of Chemically Modified Graphene: Graphene nanoplatelets (GNs, AO-2) with a specific surface area of 100 m^2 g^{-1} and 99.9% purity (purchased from Graphene Supermarket, USA) were used. Generally, the raw GNs can be prone to aggregation and precipitation in base fluids in the absence of a surfactant due to their hydrophobic properties. For better dispersion, chemically modified graphene was simply prepared via using nitric acid (HNO_3) and sulfuric acid (H_2SO_4) with concentrations of 63% and 98% (1:3 v/v), respectively.

Preparation of the Films of TOBC-IL-G: Stable aqueous TOBC dispersion with a concentration of 45 mg/10 mL was prepared by TEMPO-mediated oxidation method of BC. For the preparation of

the TOBC-IL-G composite, chemically modified graphene and TOBC aqueous suspensions were mixed together in two mixing proportions, 0.05 and 0.1 wt%, followed by stirring for 24 h at room temperature. After the stirring, 0.5 g of the [EMIM][BF_4] (1-ethyl-3-methylimidazolium tetrafluoroborate, >98%, purchased from Ionic Liquids Technologies (IOLITEC, Germany) was added to the dispersion and the TOBC-IL-G dispersion was ultrasonicated for 1 h to obtain homogeneous dispersions. The TOBC-IL-G dispersions were poured into casting devices and dried for 24 h at 65 °C in a vacuum oven. Finally, TOBC-IL-G films were dipped into the PEDOT:PSS solution to deposit electrodes on both sides of the composites; these were then dried for 3 h at 65 °C in the vacuum oven.

Characterization of TOBC-IL-G Membranes: SEM observations were conducted on a JSM-7500F (JEOL Co.), 3.0 kV microscope. The membranes were thoroughly dried in the vacuum oven before capturing the surface and cross-sectional images. The FT-IR spectra of the BC, TOBC, TOBC-IL, chemically modified graphene, and TOBC-IL-G composites were scanned using a Spectrum 400 (PerkinElmer Co.). XRD was measured using an X'Pert PRO multipurpose X-ray diffractometer, from PANalytical Co., in the range of 5°–40°. The tensile strength, modulus properties, and elongation of the BC, TOBC, BC-IL, TOBC-IL, and TOBC-IL-G composite membranes were measured using a table-top universal testing machine (AGS-X, Shimadzu Corp., Japan) equipped with a 1 kN load cell. All tested samples had dog bone shapes. The test speed was set to a rate of 10 mm min^{-1}. TGA measurements of the BC, TOBC, BC-IL, TOBC-IL, and TOBC-IL-G composite membranes were performed on a Thermogravimetric Analyzer (TG209F3) from NETZSCH (Germany) with a temperature range from 40 to 800 °C under nitrogen atmosphere conditions and at a heating rate of 10 °C min^{-1}. All membranes were air dried. Ionic liquid uptake values and swelling ratio of the BC, TOBC, and TOBC-G composites were determined by the ratios of the weights and lengths of the ionic liquid absorbed membranes and the dried one, respectively. IEC indicates the number of mill equivalents of ions in 1.0 g each of the dry BC, TOBC, and TOBC-G composite membranes. The ion exchange capacity was determined via the titration method using phenolphthalein as an indicator. The acidic form of the membrane was converted to the sodium form by immersion in 1 M NaCl solution for 24 h. The exchanged ions in the solution were titrated with a 0.1 M NaOH solution. The ionic conductivities of the BC, TOBC, and TOBC-G composite membranes incorporating deionized water and ionic liquid were calculated through the electrochemical impedance spectroscopy data obtained from a complex impedance analyzer (VersaSTAT 3 potentiostat/galvanostat, Princeton Applied Research) over a frequency range of 10–1 MHz under a maximum voltage of 20 mV. Composite membranes of circular shape with a 6 mm diameter and an ECC-STD electrochemical cell with two stainless steel electrodes were used. The specific capacitance (F cm^{-2} or F g^{-1}) in the cyclic voltammetry measurements are calculated using the following equation:

$$C_{sp} = \frac{1}{\Delta V \cdot \nu \cdot S} \int_{V_1}^{V_2} I \, dV, S = A \text{ or } m \tag{3}$$

where ΔV, ν, A, and m are the potential window, scan rate, and surface area and weight of the composite membranes, respectively.

Fabrication of Actuator and Experimental Setup for Actuation Tests: Thin PEDOT:PSS electrodes were deposited on both sides of the TOBC-IL-G membrane. The size of the actuator was 4 mm × 40 mm × 0.15 mm including an ≈4 mm × 5 mm clamping area at one end. The experimental setup of the displacement measurement consisted of National Instruments (NI) - PCI eXtensions for Instrumentation (PXI) data acquisition system (NI-PXI 6252 board), a current amplifier (UPM1503, Quanser), laser displacement sensors (OFV-303, Polytec and LK-031, Keyence), and a charged-couple device camera (XC-HR50, Sony). The measurement point was located at around 5 mm from the tip point as shown in Figure 7 (red point). So, the free length (l) of the actuator was 30 mm. All the data were acquired and controlled by an NI-PXI system (NI-PXI 1042Q) using the LabVIEW program. The generated strain was determined by the following equations.

$$\varepsilon = 2d\delta / \left(l^2 + \delta^2\right) \tag{4}$$

where d, δ, and l are the thickness, tip displacement, and the free length of the actuator, respectively.

Supporting Information

Supporting Information is available from the Wiley Online Library or from the author.

Acknowledgements

S.S.K. and J.H.J. contributed equally to this work. This work was supported by International Collaborative R&D Program through KIAT grant funded by the MOTIE (N0000894). Also, this work was supported by the Center for Advanced Soft-Electronics funded by the Ministry of Science, ICT and Future Planning as Global Frontier Project (CASE- 2011-0031640).

Received: February 16, 2015
Revised: April 8, 2015
Published online: May 5, 2015

[1] R. H. Baughman, *Science* **2005**, *308*, 63.
[2] F. Carpi, E. Smela, *Biomedical Applications of Electroactive Polymer Actuators*, John Wiley & Sons, Chichester, UK **2009**.
[3] T. Fukushima, K. Asaka, A. Kosaka, T. Aida, *Angew. Chem. Int. Ed.* **2005**, *44*, 2410.
[4] T. F. Otero, J. G. Martinez, *Adv. Funct. Mater.* **2014**, *24*, 1259.
[5] L. H. Lu, J. H. Liu, Y. Hu, Y. W. Zhang, W. Chen, *Adv. Mater.* **2013**, *25*, 1270.
[6] M. Irimia-Vladu, *Chem. Soc. Rev.* **2014**, *43*, 588.
[7] J. Lu, S. G. Kim, S. Lee, I. K. Oh, *Adv. Funct. Mater.* **2008**, *18*, 1290.
[8] G. M. Spinks, G. G. Wallace, L. S. Fifield, R. L. Dalton, A. Mazzoldi, D. De Rossi, I. I. Khayrullin, R. H. Baughman, *Adv. Mater.* **2002**, *14*, 1728.
[9] M. Rajagopalan, I. K. Oh, *ACS Nano* **2011**, *5*, 2248.
[10] C. Jo, D. Pugal, I. K. Oh, K. J. Kim, K. Asaka, *Prog. Polym. Sci.* **2013**, *38*, 1037.
[11] J. Kim, J. H. Jeon, H. J. Kim, H. Lim, I. K. Oh, *ACS Nano* **2014**, *8*, 2986.
[12] J. Kim, S. Yun, Z. Ounaies, *Macromolecules* **2006**, *39*, 4202.
[13] J. H. Jeon, I. K. Oh, C. D. Kee, S. J. Kim, *Sens. Actuators B* **2010**, *146*, 307.
[14] J. Li, S. Vadahanambi, C. D. Kee, I. K. Oh, *Biomacromolecules* **2011**, *12*, 2048.
[15] C. H. Hong, S. J. Ki, J. H. Jeon, H. Che, I. K. Park, C. D. Kee, I. K. Oh, *Compos. Sci. Technol.* **2013**, *87*, 135.
[16] J. H. Jeon, R. K. Cheedarala, C. D. Kee, I. K. Oh, *Adv. Funct. Mater.* **2013**, *48*, 6007.
[17] L. Lu, W. Chen, *Adv. Mater.* **2010**, *22*, 3745.
[18] Y. J. Choi, Y. Ahn, M. S. Kang, H. K. Jun, I. S. Kim, S. H. Moon, *J. Chem. Technol. Biotechnol.* **2004**, *79*, 79.
[19] B. R. Evans, H. M. O'Neill, V. P. Malyvanh, I. Lee, J. Woodward, *Biosens. Bioelectron.* **2003**, *18*, 917.
[20] J. Yang, D. Sun, J. Li, X. Yang, J. Yu, Q. Hao, W. Liu, J. Liu, Z. Zou, J. Gu, *Electrochim. Acta* **2009**, *54*, 6300.
[21] T. Saito, S. Kimura, Y. Nishiyama, A. Isogai, *Biomacromolecules* **2007**, *8*, 2485.

[22] S. S. Kim, J. H. Jeon, C. D. Kee, I. K. Oh, *Smart Mater. Struct.* **2013**, *22*, 085026.
[23] S. Fujisawa, Y. Okita, H. Fukuzumi, T. Saito, A. Isogai, *Carbohydr. Polym.* **2011**, *84*, 579.
[24] Z. Fang, H. Zhu, Y. Yuan, D. Ha, S. Zhu, C. Preston, Q. Chen, Y. Li, X. Han, S. Lee, G. Chen, T. Li, J. Munday, J. Huang, L. Hu, *Nano Lett.* **2014**, *14*, 765.
[25] A. Isogai, T. Saito, H. Fukuzumi, *Nanoscale* **2011**, *3*, 71.
[26] S. Nemat-Nasser, Y. X. Wu, *J. Appl. Phys.* **2003**, *93*, 5255.
[27] S. Savagatrup, E. Chan, S. M. Renteria-Garcia, A. D. Printz, A. V. Zaretski, T. F. O'Connor, D. Rodriquez, E. Valle, D. J. Lipomi, *Adv. Funct. Mater.* **2015**, *25*, 427.
[28] M. Irimia-Vladu, E. D. Glowachi, G. Voss, S. Bauer, N. S. Sariciftci, *Mater. Today* **2012**, *15*, 340.
[29] L. Martiradonna, *Nat. Mater.* **2014**, *13*, 428.
[30] A. Campana, T. Cramer, D. T. Simon, M. Berggren, F. Biscarini, *Adv. Mater.* **2014**, *26*, 3874.
[31] Y. Feng, X. Zhang, Y. Shen, K. Yoshino, W. Feng, *Carbohydr. Polym.* **2012**, *87*, 644.
[32] S. Ifuku, M. Tsuji, M. Morimoto, H. Saimoto, H. Yano, *Biomacromolecules* **2009**, *10*, 2714.
[33] S. Hestrin, M. Schramm, *Biochem. J.* **1954**, *58*, 345.
[34] T. F. Otero, J. G. Martinez, K. Hosaka, H. Okuzaki, *J. Electroanal. Chem.* **2011**, *657*, 23.
[35] F. Wang, S. S. Kim, C. D. Kee, Y. D. Shen, I. K. Oh, *Smart Mater. Struct.* **2014**, *23*, 074006.
[36] R. K. Cheedarala, J. H. Jeon, C. D. Kee, I. K. Oh, *Adv. Funct. Mater.* **2014**, *24*, 6005.
[37] C. J. Son, S. Y. Chung, J. E. Lee, S. J. Kim, *J. Appl. Microbiol. Biotechnol.* **2002**, *12*, 722.
[38] T. Isogai, T. Saito, A. Isogai, *Cellulose* **2011**, *18*, 421.